ingegneria sismica
International Journal of Earthquake Engineering
Anno XLIII - Num. 1 - 2026

Research on Real-time Dynamic Estimation Methods for Short-circuit Capacity in Distribution Networks Based on Non-perturbation Technology

Siyang He[1], *Shuai Wang*[2], *Changhong Liu*[1], *Jufeng Jin*[1], *Yonglong Gu*[1] *and Linpeng Yao*[3,*]

[1] Guizhou Power Grid Co., Ltd. Power Grid Planning and Research Center, Duyun Power Supply Bureau, Guiyang, Guizhou, 550003, China
[2] Guizhou Power Grid Co., Ltd. Power Grid Planning and Research Center, Tongren Power Supply Bureau, Guiyang, Guizhou, 550003, China
[3] Shanghai Jiao Tong University, Shanghai, 200240, China

SUMMARY: *Real-time estimation of short-circuit capacity under operational conditions holds significant practical value for assessing the stability level of distribution grids under various disturbance conditions. This paper employs the two-point method to solve circuit equations and evaluate load-saving operational states. Based on non-disturbance technology—weighted adaptive recursive least squares—the short-circuit capacity provided by connected power sources is calculated. Through simulation analysis and verification, taking a 110 kV substation in the Su North region as the research object, it can be observed that the nighttime operating mode is relatively small, while the daytime operating mode is relatively large. The non-disturbance method proposed in this paper for measuring short-circuit capacity shows that if the ratio of load capacity to actual short-circuit capacity exceeds 15%, the error will reach 10%. Therefore, this method can be further extended to address grid safety issues and holds significant research value.*

KEYWORDS: *least squares method; simulation analysis; non-disturbance technology; short-circuit capacity*

1 Introduction

With the rapid development of power systems, the safety and stability of power grids have become critical to the sustained development of the socio-economic sector. Short-circuit current calculations in distribution grids are essential for the proper selection and configuration of protective devices, serving as a key component in maintaining the safe and stable operation of power systems [1, 2]. Traditional distribution grids, characterized by unidirectional energy flow, can utilize node voltage equations to calculate short-circuit currents [3]. However, with the increasing adoption of distributed power sources, particularly in active distribution grids, short-circuit current calculations have become significantly more complex [4].

There has been a change in internal topology of distribution systems due to the continuous penetration of distributed energy sources (DERs) into them. Specifically, the conventional form of distribution systems as a single-source system has gradually evolved into a more intricate network with two or more ends [5-7]. Conversely, the conventional methods of

*ylp_sjtu@163.com
https://doi.org/10.65102/is2026489
Published: 30 April, 2026

calculating short-circuit currents are grounded on transient linear models of AC synchronous machines and networks. However, as control methods used in the inverters influence the dynamics at the interface between DERs and the location where these devices are connected, non-linear relations between output current and voltage can be observed [8-12]. Moreover, traditional methods do not apply to distribution systems with DERs because of the changes in the equivalent circuit model that is applied to the calculation of the short-circuit currents, as well as the aforementioned factors [13-16]. As the dynamics of these systems regulated by power electronic converters have significant non-linearities, the traditional methods have difficulties in being applied to short-circuit current calculations in active distribution systems [17-19].

The symmetrical component analysis is one conventional method of performing short circuit calculations, and it has been studied extensively by researchers in China and other countries. To obtain high accuracy in the definition of the state of the system and the short-circuit current, Ghanaatian, M., Lotfifard, S., et al. came up with a new algorithm to compute the short-circuit current in distribution systems with inverter-based distributed generation by combining the generalized minimal residual algorithm and the symmetrical components to solve the fault model of the distribution network [20]. van der Blij et al. eliminated imbalance issue in bipolar DC distribution system by splitting the DC system into symmetrical components and developing symmetrical domain equivalent circuit depending on the fault scenario, thus enabling estimation of the short-circuit current [21]. Castro, L., et al. developed an efficient method of short-circuit current calculation based on symmetrical elements and superconducting fault current limiter. Because of the nonlinear nature of ScFCLs, this method is particularly well suited to the calculation of short-circuit currents of radial distribution networks and meshed networks [22]. Yuan, S. et al. discovered that the photovoltaic systems of renewable energy have low-voltage ride-through ability. In the process of studying the characteristic of short-circuit current at various values of voltage drops, they obtained the RMS voltage formula under steady-state short-circuit current condition, which serves as a valuable basis of short-circuit current calculation of power grid with large-scale photovoltaics [23].

The approach of phase components is widely applied to the calculation of short-circuit currents of distribution networks since it is versatile and considers the asymmetric three-phase parameters. Zhou et al. discovered that the significant level of mutual dependency between fault mechanisms and control strategies in distribution networks alters the fault characteristics of the latter. In order to address this issue, they proposed a three-step solution to calculate the peak short-circuit currents in the distribution network using variable-structure control theory and obtained the precise estimation of the peak of the short-circuit current in the distribution network [24]. Short-circuit currents in distribution grids were examined with respect to the influence of renewable energy feed-in by Balzer. Using the variable-structure converter as the infinite internal resistance in positive sequence and computing the superposition of two current components by the superposition theorem (short circuit alternating current and fault location current) the author explored the interaction between access to renewable energy and short-circuit currents [25]. Lin et al. proposed a technique to study grid stability using measurement of impedance. They chose the D-Q frame impedance model as a conversion of distribution networks to linear time-invariant systems and therefore separated three-phase four-wire systems from single-phase loading, which may be used in short-circuit current calculations [26].

To sum up, domestic and overseas scholars have conducted research on the method of calculating the short-circuit current of distribution networks. Nevertheless, the current methods of calculation are also subject to certain shortcomings, such as the fact that they are

difficult to calculate, require complex models, do not consider the equivalent model of the distributed power source, and are prone to errors because they use a simple circuit equivalent modeling method. It is thus evident that more research needs to be done on the real-time dynamic calculation approach of short-circuit current in distribution network.

To implement the real-time dynamic computation of short-circuit capacity in distribution networks, the two-point method was chosen in this research to solve the circuit equations and determine the Thevenin parameter expression and load shedding operation condition assessment parameters are suggested. To calculate non-linear dependence between state of charge and open circuit voltage and thus obtain the short circuit capacity of power source connected to distribution network, non perturbation recursive least squares method is applied. The algorithm presented in the current paper will be analyzed based on the error analysis and simulation analysis under the condition of various short-circuit capacities using 110 kV substation of SuNorth Region as an example.

2 Real-time dynamic estimation method for short-circuit capacity in distribution networks based on non-perturbation technology

2.1 Calculation of short-circuit capacity

Short-circuit capacity is an indicator of node voltage strength, reflecting the voltage stability and load-carrying capacity of the node. When load node i is connected to a new power source, the equivalent circuit of Davenport facing load node i [27].

The equivalent potential is $\dot{E}_T$, the phase angle is 0, the equivalent impedance is $Z_T = R_T + jX_T$, the connected power source is $\dot{E}_{DG}$, the equivalent impedance of the power source is Z_{DG}, and the active and reactive powers of the newly connected power source are P_{DG}, Q_{DG}. The voltage amplitude and phase angle of load node i are U_L, θ. The load power is $\dot{S}_L = P_L + jQ_L$.

According to the definition, the required short-circuit capacity of load node i:

$$S_{sc-i} = \frac{U_L^2}{|Z_L|} \tag{1}$$

Define the short-circuit capacity available on the system side at node i:

$$S_{sc}^{'} = \frac{E_T^2}{|z_T|} \tag{2}$$

When not connected to a power source, there is a load of $\dot{E}_{DG} = 0$ at the load node, i.e., $S_{sc}^{''} = 0$.

When the load node is connected to the power supply, there are:

$$S_{sc}^{"} = \frac{E_{DG}^2}{|z_{DG}|} \tag{3}$$

The total short-circuit capacity that the system and power supply can provide is:

$$\overline{S}_{sc} = S'_{sc} + S''_{sc} \tag{4}$$

By comparing the required short-circuit capacity of load node i with the actual short-circuit capacity required by the load node, the operating status of the load node can be identified. The operating status indicator ω_{ni} of the load node is defined as:

$$\omega_{r_i} = \frac{S_{sc_i}}{\overline{S}_{sc}} \tag{5}$$

2.2 Evaluation method for load power saving operation status

Using the two-point method, the analytical expressions for the Thevenin parameters are derived by solving the circuit equations, and the Thevenin parameters are calculated directly. According to a certain migration law, only the magnitude of the active power and reactive power at the observed load node is changed, while strictly maintaining the power at other nodes in the power grid and the operating mode and topological structure of the system unchanged, so that the operating domain point at the observed load node can be obtained [28].

By calculating power flows and conducting real-time monitoring, initial operating point and domain point node voltage and load current data can be obtained at load node i. The node voltage and current of the operating point and its neighboring points are represented by $V_0\angle\varphi_{t0}, I_0\angle\varphi_{t0}$ and $V_1\angle\varphi_{v1}, I_l\angle\varphi_{l1}$, respectively.

Assuming that the operating point to domain point The Davenport parameters remain unchanged, according to circuit theory:

$$\begin{cases} E_T e^{j\psi_T} = I_0 Z_T e^{j(\varphi_{l0}+\varphi_T)} + V_0 e^{j\varphi_{t0}} \\ E_T e^{j\psi_T} = I_1 Z_T e^{j(\varphi_{l1}+\varphi_T)} + V_1 e^{j\varphi_{v1}} \end{cases} \tag{6}$$

By derivation, the analytical expressions for the four parameters of the node network under test, namely the equivalent impedance modulus Z_r, equivalent impedance angle φ_T, equivalent potential impedance angle ψ_r, and equivalent potential E_r, can be obtained. Among them:

$$Z_T = \frac{V_1 \cos\varphi_{V1} - V_0 \cos\varphi_{V0}}{\beta\cos\varphi_T - \alpha\sin\varphi_T} \tag{7}$$

$$E_T = I_0\sqrt{(R_T + R_L)^2 + (X_T + X_L)^2} \tag{8}$$

2.3 Calculation method for short-circuit capacity provided by the power supply

When selecting a synchronous motor model as the power supply model, its parameters are shown below. Generator equivalent potential modulus:

$$E_G = \sqrt{(V + Ix_q\sin\varphi)^2 + (Ix_q\cos\varphi)^2} \tag{9}$$

Equivalent impedance of generator:

$$Z_G = jx_q \tag{10}$$

The short-circuit capacity that a single synchronous generator set can provide is $S_{sc}^{"}$, so we have:

$$S_{sc}^{"} = \frac{(E_G)^2}{|Z_{eq}|} \tag{11}$$

Open circuit voltage is the precise parameter that can describe the state of charge (SOC) of lithium-ion battery cells within the second-order RC equivalent model. There is a non-linear relationship between SOC and OCV which may be derived using the SOC-OCV graph.

This non-linear mapping can be obtained experimentally. The procedure is described below: put the ambient temperature to 25C, charge and discharge the cell at 0.2C until it increases its capacity by 0.1 C, hold on 10 minutes, and then keep charging or discharging until the voltage has reached the threshold level of charging/discharging.

This paper involves experimentation on a single-cell lithium-ion battery and data concerning SOC and OCV at both charging and discharging have been gathered. To this end, mean OCV values at each SOC were taken as the ultimate values to be applied in non-linear fitting of the graph. A polynomial order of 6 to 9 was found to be appropriate for the curve fitting. When the order is too low, the curve details are not well handled, resulting in poor accuracy. When the order is too high, overfitting issues may arise. After multiple experiments, this study adopted an 8th-order fit.

The fitted 8th-order polynomial equation is:

$$\begin{aligned} f(z) &= 245.5362z^8 - 843 - 8467z^7 + 1074.4691z^6 - 533.4221z^5 \\ &-61.9175z^4 + 185.1491z^3 - 80.6698z^2 + 15.1314z + 2.2255 \end{aligned} \tag{12}$$

After obtaining the SOC-OCV relationship, the weighted adaptive least squares method is used to identify the parameters of the established battery equivalent model. The process is as follows:

Laplace transform:

$$U_{oc}(s) - U(s) = \left(R_0 + \frac{R_1}{1 + R_1 C_1 s} + \frac{R_2}{1 + R_2 C_2 s} \right) I(s) \tag{13}$$

With the difference between the open-circuit voltage and the terminal voltage Laplace transform $(U_{oc}(s) - U(s))$ as the input, and the charge-discharge current Laplace transform $I(s)$ as the output, the transfer function of this model is:

$$G(s) = \frac{(R_0 + R_1 + R_2) + (R_0\tau_1 + R_0\tau_2 + R_1\tau_2 + R_2\tau_1)s + R_0\tau_1\tau_2 s^2}{1 + (\tau_1 + \tau_2)s + \tau_1\tau_2 s^2} \tag{14}$$

Parameter identification is based on discrete sampling data, so equation (8) is transformed bilinearly according to equation (9):

$$s = \frac{2}{T} \cdot \frac{1 - Z^{-1}}{1 + Z^{-1}} \tag{15}$$

In the formula, $Z = e^{Ts}$ is the Z transformation operator. T is the sampling period. s is the Laplace transformation operator.

The discrete transfer function of the model is obtained as:

$$G(Z^{-1}) = \frac{a_3 + a_4 Z^{-1} + a_5 Z^{-2}}{1 - a_1 Z^{-1} - a_2 Z^{-2}} \tag{16}$$

Equation (10) can be written in the form of a difference equation as follows:

$$y(k) = a_1 y(k-1) + a_2 y(k-2) + a_3 I(k) + a_4 I(k-1) + a_5 I(k-2) \tag{17}$$

In the equation, $a_1 \sim a_5$ are undetermined coefficients; $y(k)$ is the difference between the open-circuit voltage and the terminal voltage at the k sampling time.

For convenience, let us write equation (11) in vector form:

$$\begin{cases} y(k) = \varphi(k)\theta(k) \\ \varphi(k) = \begin{bmatrix} y(k-1) & y(k-2) & I(k) & I(k-1) & I(k-2) \end{bmatrix} \\ \theta(k) = \begin{bmatrix} a_1 & a_2 & a_3 & a_4 & a_5 \end{bmatrix}^T \end{cases} \tag{18}$$

When equation (12) is put into matrix notation and recursive least squares (RLS) algorithm is employed, the criterion function will be considered to be the sum of squared errors, and the recursive formula can be obtained as follows:

$$\begin{cases} \theta(k) = \theta(k-1) + K(k)[y(k) - \varphi(k-1)\theta(k-1)] \\ P(k) = [I - K(k)\varphi(k-1)]P(k-1) \\ K(k) = \dfrac{P(k-1)\varphi^T(k-1)}{1 + \varphi(k-1)P(k-1)\varphi^T(k-1)} \end{cases} \tag{19}$$

In the formula, $\theta(k)$ is the parameter estimation matrix. $P(k)$ is the covariance matrix. $K(k)$ is the gain matrix. I is the unit matrix.

The use of RLS technique helps reduce the effect of uncertainties that exist in the environment on the modeling process as well as the system parameters by updating these parameters periodically. However, in situations where there is slow time variation of parameters of the system, the accuracy in identifying these parameters becomes difficult with RLS technique. For this reason, weighted adaptive recursive least squares method (WARLS) is considered in the present research paper for parameter identification. With the use of adaptive weight factor, the relative importance of old data against new data in the recursive technique can be controlled.

The weighted adaptive recursive equation is:

$$\begin{cases} \lambda(k)=1-\dfrac{1}{1+\varphi(k-1-l)P(k-1)\varphi^T(k-1-l)}\dfrac{e^2(k)}{r} \\ \theta(k)=\theta(k-1)+K(k)[\gamma(k)-\varphi(k-1)\theta(k-1)] \\ K(k)=\dfrac{P(k-1)\varphi^T(k-1)}{\lambda(k)+\varphi(k-1)P(k-1)\varphi^T(k-1)} \\ P(k)=\dfrac{1}{\lambda(k)}[-K(k)\varphi(k-1)]P(k-1) \end{cases} \tag{20}$$

In the formula, $\lambda(k)$ is the adaptive weighting factor; l,r is the weighting adjustment coefficient, which is adjusted according to the estimated error $e(k)=y(k)-\varphi(k-1)\theta(k-1)$. When the error increases, the weighting factor decreases; when the error decreases, the weighting factor increases.

The corresponding coefficients are equal, resulting in the model parameter identification equation:

$$\begin{cases} \tau_1+\tau_2=\dfrac{1+a_2}{1-a_1-a_2}\cdot T \\ T_1\tau_2=\dfrac{1+a_1-a_2}{1-a_1-a_2}\cdot\dfrac{T^2}{4} \\ R_0+R_1+R_2=\dfrac{a_3+a_4+a_5}{1-a_1-a_2} \\ R_0\tau_1+R_0\tau_2+R_1\tau_2+R_2\tau_1=\dfrac{a_3-a_5}{1-a_1-a_2}\cdot T \\ R_0\tau_1\tau_2=\dfrac{a_3-a_4+a_5}{1-a_1-a_2}\cdot\dfrac{T^2}{4} \end{cases} \tag{21}$$

Equation (15) can be used to obtain an equivalent model of a lithium-ion battery. Using this model, different estimation methods can be employed to estimate parameters such as the battery's state of charge (SOC).

3 Simulation Analysis and Verification

Taking a 110 kV substation in northern Jiangsu Province as an example, its system connection is shown in Figure 1.

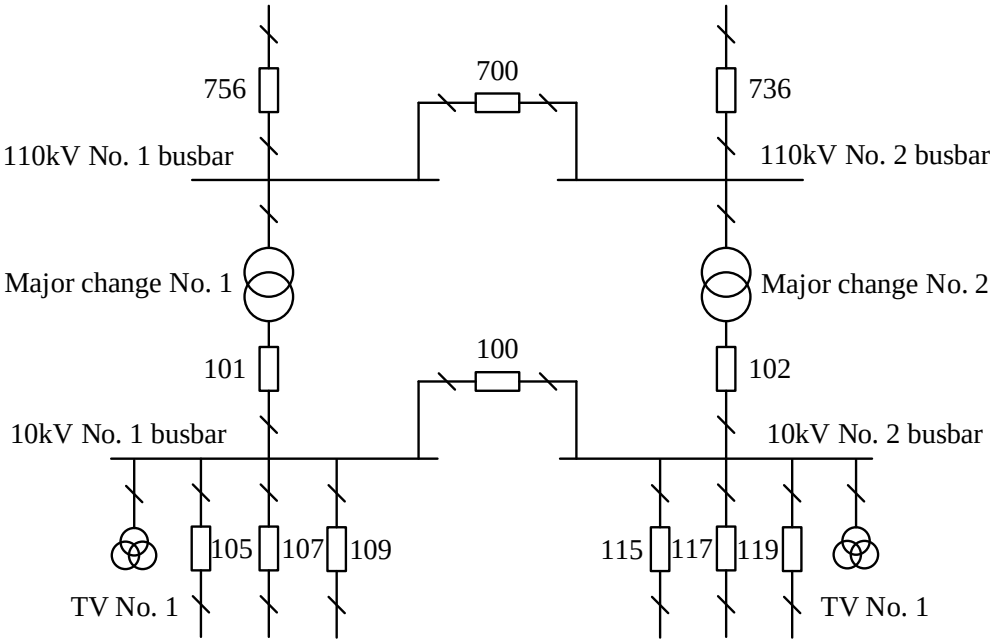

Figure 1: System connection

3.1 Error Analysis of the Algorithm

According to the "Annual Regional Power Grid Relay Protection Setting Plan and Dispatch Operation Guidelines," the nominal values of the system impedance for the 10kV Bus No. 2 at a certain 110kV substation under maximum and minimum operating conditions are 0.26/0.48 Ω, respectively. If S_B is taken as 100 MV·A, and U_B is 10.7 kV, then the relationship between the unit impedance's nominal value Z^* and the nominal value is:

$$Z_B = \frac{U_B^2}{S_B} = \frac{10.7^2}{100} = 1.1449\Omega \tag{22}$$

Thus, the system impedance values of the 10kV busbar in the maximum/minimum modes are as follows:

$$Z_{\max}* = \frac{Z_{\max}}{Z_B} = 0.23567\,p.u. \tag{23}$$

$$Z_{\min}* = \frac{Z_{\min}}{Z_B} = 0.42645\,p.u. \tag{24}$$

As can be seen from the busbar voltage fluctuations caused by the switching of capacitors at the 110 kV substation on a certain day, after the capacitor bank was switched on at 13:45, the voltage of the 10 kV No. 2 busbar at the 110 kV substation rose from 10.17 kV to 10.30 kV: After the capacitor was disconnected at 22:15 on the same day, the busbar voltage decreased from 10.45 kV to 10.29 kV. Given that the rated capacity of the capacitor bank associated with the 10kV Bus No. 2 at this substation is 4500kV, if the changes in grid parameters under the capacitor engagement scenario are used as the basis for calculation, then the short-circuit capacity of the 10kV Bus No. 2 at this substation can be estimated using Equation (11):

$$S_{d\_T}^{'} = 354MV \cdot A \tag{25}$$

The system impedance magnitude value corresponding to the operating mode at that time is:

$$Z_{XT1}* = \frac{S_B}{S_d} = 0.28411 p.u. \tag{26}$$

Obviously, $Z_{XT1}* \in [0.23567, 0.42645]$, i.e., the current operating mode, is within the operating mode specified in the "Annual Regional Power Grid Relay Protection Setting Plan and Dispatch Operation Instructions" and is consistent with the actual operating conditions.

If the changes in grid parameters under capacitor removal are used as the basis for calculation, then the short-circuit capacity of the 10kV No. 2 busbar of the substation is:

$$S_{d\_Q}^{'} = 290MV \cdot A \tag{27}$$

The system impedance magnitude value corresponding to the operating mode at that time is:

$$Z_{XT2}* = \frac{S_B}{S_d} = 0.345544 p.u. \tag{28}$$

The operating modes are shown in Figure 2. It is easy to see that the nighttime operating mode is smaller, while the daytime operating mode is larger, which is consistent with the actual operating conditions of the power grid.

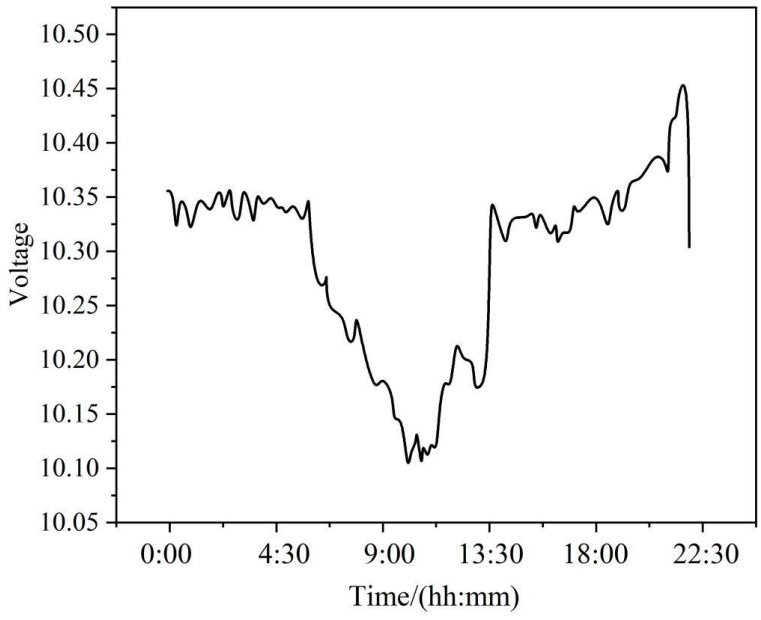

Figure 2: The line voltage engraving curve before and after the capacitor

Still using the above case as a background, the measured current curve of the 10kV No. 2 busbar capacitor of the substation is shown in Figure 3.

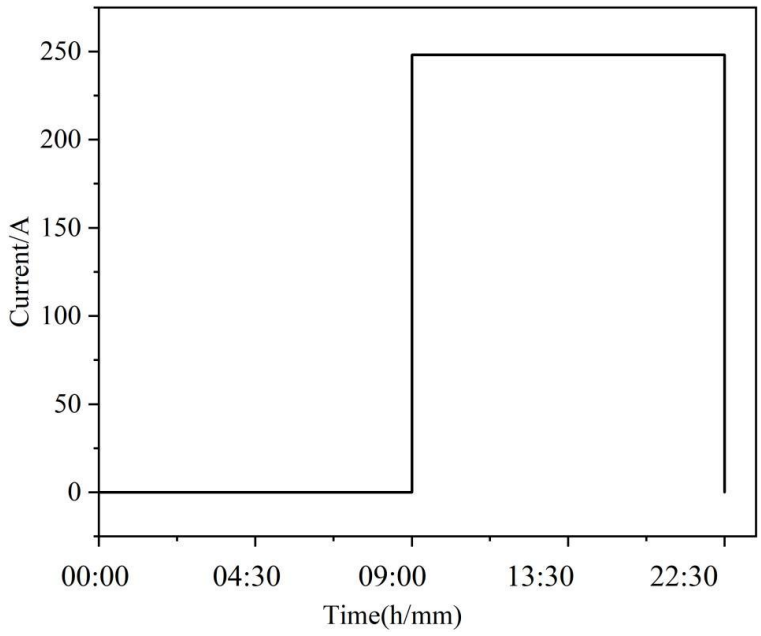

Figure 3: The current curve of the capacitor before and after the capacitor is cut

Because the busbar voltage has a certain correlation with the output capacity of the capacitor, it will be better to calculate the real output capacity of the capacitor based on the measured voltage and current of the capacitor itself. After the capacitor bank was energized at 13:45, the phase current of the capacitor was 251.56 A. Before the capacitor bank was disconnected at 22:15, the phase current of the capacitor was 254.78 A. Therefore, the busbar short-circuit capacity when the capacitor bank was energized is:

$$S_{d\_T}^{*} = 353MV \cdot A \tag{29}$$

The busbar short-circuit capacity under the capacitor removal method is:

$$S_{d\_Q}^{*} = 298MV \cdot A \tag{30}$$

Comparing the calculation results of $S_{d\_T}^{'}, S_{d\_Q}^{'}$ and $S_{d\_T}^{*}, S_{d\_Q}^{*}$, the voltage variation value is:

$$\Delta U = U_{S1} - U_{S0} = 0.14kV \tag{31}$$

If the vector method is used, then:

$$\Delta \dot{U} = \dot{U}_{S1} - \dot{U}_{S0} \tag{32}$$

Comparing the calculation results, it can be seen that the impact caused by changes in capacitor output capacity due to busbar voltage is negligible. In engineering calculations, using the rated capacity of the capacitor directly can meet the requirements of practical applications. Additionally, US0 and US1 in Equation (11) should both be vectors; however, vector calculations are relatively complex in engineering applications. Therefore, all examples in this paper use scalar calculation methods. Whether the resulting errors significantly affect the calculation results, both theoretical analysis and actual operational conditions indicate that

under normal load variations, the power angle difference of the busbar voltage generally does not exceed 6°. Using the aforementioned example as a backdrop, under capacitor operation mode, the voltage variation values calculated using the scalar method are shown in Figure 4.

As can be seen from the figure, when the angle is less than 0.2°, the calculation errors of the two algorithms are very small. However, as the angle increases, the errors also increase significantly. When the angle is 0.5°, the calculation error reaches 16%. The conclusion is that the reduction of the voltage angles difference between the initial and final stage of the operation change can be achieved through the computation of accurate results. According to the concepts of power system analysis, the angle difference of the voltages of different operation conditions is proportional to the change in the active power produced by the busbar. In the aforementioned example, the active power output from the busbar before and after the capacitor was connected was 15.27 MW and 15 MW, respectively. Similarly, before and after the capacitor was disconnected, the active power output from the busbar was 17.82 MW in both cases, with almost no change, indicating that the results have good computational accuracy and align with engineering practice.

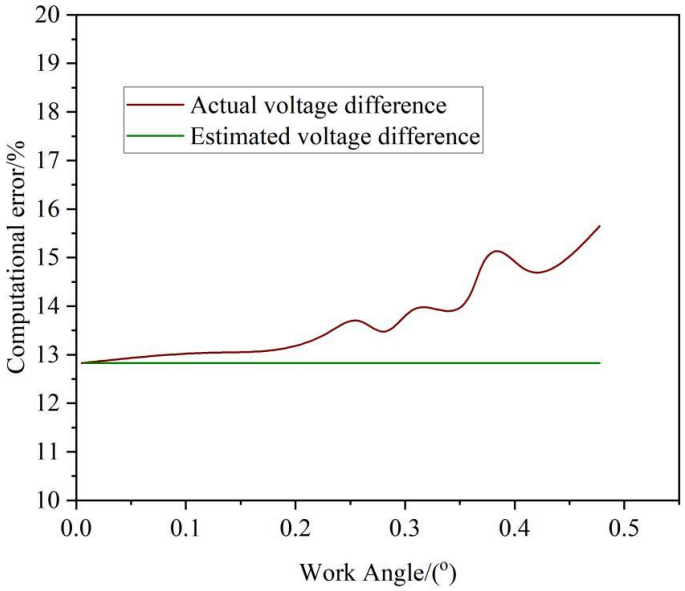

Figure 4: Error of voltage difference between vector and scalar method

3.2 Simulation analysis of different short-circuit capacity levels

In order to test the suitability of the non-disturbance approach proposed in this paper, the values of the short-circuit capacity were selected as 200 MVA and 1,500 MVA. The results of the simulation with various parameters are given in Table 1.

As you can see in Table 1, the largest measurement error is 2%. It implies that it is a simulation error created under extreme conditions where the short-circuit capacity parameter is 200 MVA - a value near to the load MVA. The result confirms that the measurement technology proposed in this work will guarantee extremely precise outcomes even in normal and exceptional situations.

Considering its contribution relative to other writings, one may note that here is a considerable difference. This is due to the suggested measurement principle, which will be to introduce the phase angle between the bus voltages before and after disturbance. Previous research work had performed all calculations based on the variations in voltage, which was very flawed and could not take into account the effects of the load currents on the bus connections. According to the simulations, if the ratio of load capacity to real short-circuit

capacity exceeds 15 percent, the error of traditional technologies is 10 percent. Therefore, the non-disturbance short-circuit capacity measuring method proposed in this paper solves much of the problem and is highly practical.

Table 1: Analysis and simulation test results

S/MVA	θ/(°)	ΔU/V	S/MVA	Δ/%
1500	0.2285	388.8	1508	-0.64
1000	0.3812	563.4	998.7	-0.26
800	0.5226	689.5	800.9	-0.05
700	0.6339	768.9	700.5	0.10
600	0.8047	870.6	603.8	0.26
500	1.0522	1005	504.8	0.45
400	1.478	1184	403.8	0.78
300	2.216	1389	303.8	1.25
200	3.682	1608	205	2.08

The voltage stability of each bus node in the model was assessed, and the results are shown in Table 2.

Analysis of the values in the table shows that node 2 has the lowest voltage stability index of only 0.0324, which means that this node has a strong load-bearing capacity and the best voltage stability. Node 1 has a voltage stability index of 0.3552, which is the highest among the nodes tested, indicating that it has the least stable voltage.

Table 2: The voltage stability evaluation of each node short circuit capacity

Waiting node	R	Voltage stability sort
1	0.3552	1
2	0.0324	5
3	0.1156	4
4	0.3389	2
5	0.2478	3

Comparison of the voltage stability indicators calculated with the help of the continuous power flow method and the indicators obtained through measuring the short circuit capacity of each node are given in Table 3.

It is also possible to find that the indicators of voltage stability assessment of the grid busbar voltages measured by the short circuit capacity proposed in this paper are consistent with the indicators of assessment of each node measured by the continuous power flow method. The agreement also substantiates the effectiveness of the proposed approach. It is worth noting that the continuous power flow method has stringent convergence limits on voltages and it is quite challenging to compute. Nevertheless, the proposed voltage stability assessment approach of the power grid busbars based on the measured short circuit capacity does not suffer the convergence issue when solving the power flow equation and therefore offers a relatively easy solution method with acceptable assessment indicators.

Table 3: The results of the voltage stability of each node were compared

Waiting node	V_1/kV	V_2/kV	τ_i	T_i Index sort	R Index sort
1	1.382	1.289	0.064	1	1
2	1.416	1.357	0.042	5	5
3	1.448	1.384	0.048	4	4
4	1.369	1.277	0.062	2	2
5	1.387	1.302	0.0574	3	3

4 Conclusion

The techniques employed in the current paper involve non-perturbation-based methods that are based on the weighted adaptive recursive least square and two-point technique of estimating the short circuit capacity and voltage stability index in distribution systems in real time. According to an error analysis and simulations, it may be concluded that the night operating mode of a substation of 110 kV in the Subei region is relatively smaller compared to the day operating mode that is relatively larger and is consistent with the operating mode of the power system. The maximum error that will be generated irrespective of the value of the short circuit capacity will not go beyond 2 percent.

Funding

This work was supported by China Southern Power Grid Science and Technology Projects Research on the Development and Practical Application of a Domestic Real-time Local Measurement Device for Grid Short-circuit Parameters (GZKJXM20220068)

About the Author

Siyang He, Master, Electrical Engineering and Automation, Guizhou Power Grid Co., Ltd. Duyun Power supply Bureau, No. 22 Doupengshan Road, Duyun Power supply Bureau, Guizhou Power Grid Co., Ltd.

Shuai Wang, junior college, senior engineer, highvoltage technology, Guizhou Power Grid Co., Ltd. Tongren Power supply Bureau, Old Building of Tongren Power supply Bureau, No. 63 Qingshui Avenue, Bijiang District, Tongren City, Guizhou Province

Changhong Liu, Bachelor's degree, Senior Engineer, Main research direction: Electrical Engineering and Automation

Linpeng Yao, PhD, researcher, Main research direction: Electrical Engineering and Automation

References

[1] Gkavanoudis, S. I., Tampakis, D., Malamaki, K. N. D., Kryonidis, G. C., Kontis, E. O., Oureilidis, K. O., ... & Demoulias, C. S. (2020). Protection philosophy in low short-circuit capacity distribution grids with high penetration of converter-interfaced distributed renewable energy sources. IET Generation, Transmission & Distribution, 14(22), 4978-4988.

[2] Katyara, S., Staszewski, L., Musavi, H. A., & Soomro, F. (2017). Short circuit capacity:

A key to design reliable protection scheme for power system with distributed generation. International Journal of Mechanical Engineering and Robotics Research, 6(2), 126-133.

[3] Strezoski, L., Prica, M., & Loparo, K. A. (2016). Generalized Δ-circuit concept for integration of distributed generators in online short-circuit calculations. IEEE Transactions on Power Systems, 32(4), 3237-3245.

[4] Sun, P., Gong, C., Du, X., Luo, Q., Wang, H., & Zhou, L. (2017). Online condition monitoring for both IGBT module and DC-link capacitor of power converter based on short-circuit current simultaneously. IEEE Transactions on Industrial Electronics, 64(5), 3662-3671.

[5] Tristiu, I., Bulac, C., Costinas, S., Toma, L., Mandiş, A., & Zăbavă, T. (2015, May). A new and efficient algorithm for short-circuit calculation in distribution networks with distributed generation. In 2015 9th International Symposium on Advanced Topics in Electrical Engineering (ATEE) (pp. 816-821). IEEE.

[6] Thurner, L., Scheidler, A., Schäfer, F., Menke, J. H., Dollichon, J., Meier, F., ... & Braun, M. (2018). pandapower—an open-source python tool for convenient modeling, analysis, and optimization of electric power systems. IEEE Transactions on Power Systems, 33(6), 6510-6521.

[7] Von Meier, A., Stewart, E., McEachern, A., Andersen, M., & Mehrmanesh, L. (2017). Precision micro-synchrophasors for distribution systems: A summary of applications. IEEE Transactions on Smart Grid, 8(6), 2926-2936.

[8] Kersting, W. H. (2018). Distribution system modeling and analysis. In Electric power generation, transmission, and distribution (pp. 26-1). CRC press.

[9] Zhang, L., & Ruan, X. (2019). Control schemes for reducing second harmonic current in two-stage single-phase converter: An overview from DC-bus port-impedance characteristics. IEEE Transactions on Power Electronics, 34(10), 10341-10358.

[10] Sun, Y., Chen, J., Qiu, R., & Li, C. (2024). Open-Circuit, Current Sensor Fault Diagnosis of Three-Phase Four-Wire Inverters Based on Fourier Fitting. IEEE Transactions on Instrumentation and Measurement.

[11] Sharaf, H. M., Zeineldin, H. H., Ibrahim, D. K., & Abou El-Zahab, E. E. D. (2015). A proposed coordination strategy for meshed distribution systems with DG considering user-defined characteristics of directional inverse time overcurrent relays. International Journal of Electrical Power & Energy Systems, 65, 49-58.

[12] Zhang, Y., Zhang, Y., Pan, X., Zhao, B., He, J., Han, Y., ... & Ye, J. (2022). Equivalent modeling method of induction motor contribution to short-circuit current. Energy Reports, 8, 1202-1210.

[13] Qi, Y., Bostanci, E., Gurusamy, V., & Akin, B. (2018). A comprehensive analysis of short-circuit current behavior in PMSM interturn short-circuit faults. IEEE Transactions on Power Electronics, 33(12), 10784-10793.

[14] Gao, S., Ye, H., & Liu, Y. (2019). Accurate and efficient estimation of short-circuit

current for MTDC grids considering MMC control. IEEE Transactions on Power Delivery, 35(3), 1541-1552.

[15] Kim, I. (2019). Short-circuit analysis models for unbalanced inverter-based distributed generation sources and loads. IEEE Transactions on Power Systems, 34(5), 3515-3526.

[16] Liang, Z., Lin, X., Kang, Y., Gao, B., & Lei, H. (2017). Short circuit current characteristics analysis and improved current limiting strategy for three-phase three-leg inverter under asymmetric short circuit fault. IEEE Transactions on Power Electronics, 33(8), 7214-7228.

[17] Zhang, F., Xin, H., Wu, D., Wang, Z., & Gan, D. (2018). Assessing strength of multi-infeed LCC-HVDC systems using generalized short-circuit ratio. IEEE Transactions on Power Systems, 34(1), 467-480.

[18] Micev, M., Ćalasan, M., Aleem, S. H. A., Hasanien, H. M., & Petrović, D. S. (2021). Two novel approaches for identification of synchronous machine parameters from short-circuit current waveform. IEEE Transactions on Industrial Electronics, 69(6), 5536-5546.

[19] Pei, X., Tang, G., Zhang, S., Xie, S., Wu, Y., & Yang, J. (2018). Analysis on transient characteristics of short-circuit current for bipolar VSC-based DC grid. Journal of Global Energy Interconnection, 1(4), 404-412.

[20] Ghanaatian, M., & Lotfifard, S. (2019). Sparsity-based short-circuit analysis of power distribution systems with inverter interfaced distributed generators. IEEE Transactions on Power Systems, 34(6), 4857-4868.

[21] van der Blij, N. H., Ramirez-Elizondo, L. M., Spaan, M. T., & Bauer, P. (2017). Symmetrical component decomposition of DC distribution systems. IEEE Transactions on Power Systems, 33(3), 2733-2741.

[22] Castro, L. M., Guillen, D., & Trillaud, F. (2018). On short-circuit current calculations including superconducting fault current limiters (ScFCLs). IEEE Transactions on Power Delivery, 33(5), 2513-2523.

[23] Yuan, S., Yang, B. F., & Zhang, J. Y. (2022). Experimental study on short-circuit current characteristics of a photovoltaic system with low voltage ride through capability under a symmetrical fault. Energy Reports, 8, 4502-4511.

[24] Zhou, N., Wu, J., & Wang, Q. (2018). Three-phase short-circuit current calculation of power systems with high penetration of VSC-based renewable energy. Energies, 11(3), 537.

[25] Balzer, G. (2016, October). Short-circuit calculation with fullsize converters according to iec 60909. In 21 st Conference of Electric Power Supply Industry, CEPSI.

[26] Lin, Q., Wen, B., Burgos, R., Li, X., Wang, Q., & Li, X. (2023). DQ impedance modeling and stability analysis of a three-phase four-wire system with single-phase loads. IEEE Transactions on Power Electronics, 38(9), 11169-11182.

[27] Siyang He, Shiqin Zhao, Shuai Wang, Juncheng Huang, Changzi Zhang & Huaiyuan Wang. (2024). A fast short circuit capacity calculation model based on regression neural network in complex grid environment. Applied Mathematics and Nonlinear Sciences,9(1).

[28] Wang Zhongrui, Xu Yonghai, He Sheng, Yuan Jindou, Yang Heng & Pan Mingming. (2023). A non-intrusive method of industrial load disaggregation based on load operating states and improved grey wolf algorithm. Applied Energy,351.